Int. J. Bio-Inorg. Hybr. Nanomater., 8(1): 39-45, Spring 2019

$CuMn_2O_4$ nanostructures: Facial synthesis, structural,magnetical, electrical characterization and activation energy calculation

M. Enhessari[1,], S. A. Lachini[2]*

[1] *Department of Chemistry, Naragh branch, Islamic Azad University, Naragh, Iran*
[2] *Department of Chemistry, Mahabad Branch, Islamic Azad University, Mahabad, Iran*

Received: 14 November 2018; Accepted: 16 January 2019

ABSTRACT: The work is the report about stearic acid sol-gel synthesis method, magnetically, electrical characterization and activation energy of copper manganese oxide nanostructures. The $CuMn_2O_4$ nanostructures are synthesized at a temperature of 600°C using the sol-gel method. The structural analysis using X-ray diffraction (XRD) and Scherrer equation show that the crystallite size of $CuMn_2O_4$ is about 23.0 nm. The activation energy value is measured by temperature-programmed reduction (TPR) analysis at three heating rates of 10, 15 and 20 °C/min and Kissinger equation .The Ea value is 28.1 kJ/mol. Vibrating sample magnetometer (VSM) analysis of the nanostructures indicates moderate ferromagnetic properties. Examination of the dielectric properties by the LCR meter indicates the semiconducting property of the nanostructure. The highest conductivity increase was in the frequency of 308 MHz equal to 70.7 μS. Therefore, the $CuMn_2O_4$ nanostructures are potential candidates in fuel cells, telephones, loudspeakers and transformers due to their properties and convenience, non-toxic and environmentally friendly production methods.

Keywords: *Activation Energy; CuMn2O4 Nanostructures; Electrical Properties; Ferromagnetism; Kissinger Equation.*

INTRODUCTION

Knowledge of solid-state materials in chemistry is essential to understand the importance of many advanced materials [1,2]. The unique physicochemical properties of advanced nano-materials, their ultra-small size, high reactivity and large surface area-to-mass ratio, have made them distinct from other materials [3]. The general formula of spinel oxides is as AB_2O_4 [4] structures with this formula show a variety of applications in electronics, magnetic materials and catalysts [5]. In $CuMn_2O_4$ normal spinel, the electron configuration of Mn^{3+} is as $3d^4$ and the electron configuration of Cu^{2+} is $3d^9$, which occupy the tetrahedral and octahedral sites, respectively. The researchers have prepared a degraded tetragonal-spinel structure using a single-step method, and measured the magnetization with respect to temperature and magnetic field [6]. In addition, they synthesized $CuMn_2O_4$ nanopowders using a low-temperature mixing technique; the mean size of the synthesized nanostructures was about 50 nm [7]. Recently, the structure, morphology and magnetic properties of $CuMn_2O_4$ have been studied [8, 9]. $CuMn_2O_4$ spinel has been used as a protective coating on a solid oxide fuel cell and compared to layered compounds such as $LiNiO_2$ and $CuCO_2$ [10]. In addition, the $CuMn_2O_4$

(*) Corresponding Author - e-mail: enhessari@gmail.com

spinel has an economic and environmental advantage as a fuel cell process [11].The $CuMn_2O_4$ nanostructures have semiconducting properties and can be used in the electronics industry. There are several methods for preparation of nanostructures such as combustion method [12], melting technique [13], chemical vapor deposition [14], atomic layer deposition [15], sol-gel [16], hydrothermal [17] and ceramic method [18].

The sol-gel method was first used historically for building and decorative materials, and then was widely used for different fields such as glasses, ceramics, catalysts, coatings, composites and fibers in the last century [19]. The sol-gel process has been applied as a versatile method for preparation of inorganic compounds and chemical materials. This method contains advantages of easy components adjustment, chemical homogeneity, low cost and low calcination temperature [20].

Preparation of $CuMn_2O_4$ nanostructures by sol-gel method was the most important challenge in this study. The nanopowders were synthesized after calcination at 600°C. Various methods containing X-ray diffraction (XRD), temperature-programmed reduction (TPR), vibrating-sample magnetometer (VSM) and LCR meter were used for study of the nanostructures. Using the techniques structural properties, activation energy, kinetic properties, magnetic behavior and electrical properties of $CuMn_2O_4$ nanostructures were investigated.

EXPERIMENTAL

MATERIALS AND METHOD

In the present study, the $CuMn_2O_4$ nanostructures were prepared by sol-gel method using stearic acid as complex agent, copper and manganese acetate as metal cation sources. The metal cations penetrate from the aqueous phase to the organic phase over the melting point of stearic acid. First, 0.3 mol stearic acid (97% purity, Merck) was melted in a beaker at 73°C. Then, in a stoichiometric ratio of 0.5 mol Cu (II) acetate (99.9% purity, Aldrich) and 0.1 mol of Mn (II) acetate (99.9% purity, Aldrich) were dissolved in water and added to molten stearic acid. At this stage, the two soluble phases became a gel. Finally, the resulting gel contained Cu (II) and Mn (II) ions. The gel was heated to boiling point of stearic acid at 100 to 350°C for 1 h until an aqueous phase was formed. Then, the resulting material was heated to 600°C for 4 h for calcination process. Finally, the material was ground in a mortar and prepared to identify its structure and properties.

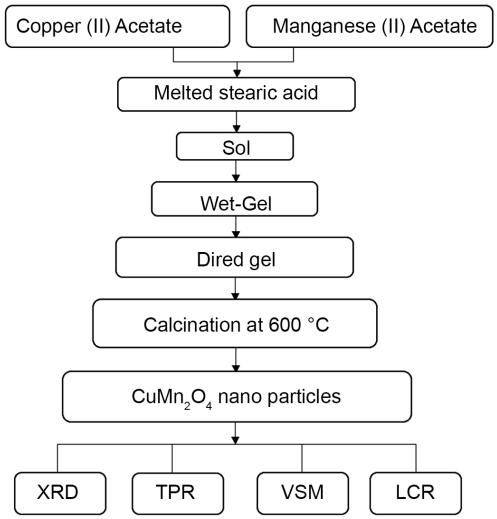

Scheme 1. Schematic illustration of $CuMn_2O_4$ nanostructures synthesis steps.

CHARACTERIZATION

XRD pattern of $CuMn_2O_4$ nanopowders was evaluated with PTF 3003 model from SEIFERT spectrometer using Cu-Kα beam (λ = 1.418Å, 30 kV and 30 mA) in range of (2θ =10°- 80°) to determine structure and size of the nanostructures (JCDPS 74-1921). Typical degradation processes were investigated using TPR technique by a thermal conductivity detector (TCD) of a gas chromatograph (6890 plus, Toseye Hesgarsazan Asia Co., Iran). The kinetic parameters were studied using adsorption/desorption isotherms of N_2 at 196 °C using Chem-BET Pulsar TPR/TPD/BET (Toseye Hesgarsazan Asia Co., Iran).

RESULT AND DISCUSSION

Structural analysis of $CuMn_2O_4$ nanostructures

XRD pattern (Fig. 1) showed the cubic structure of $CuMn_2O_4$ nanopowders with space group */Fd-3 m.

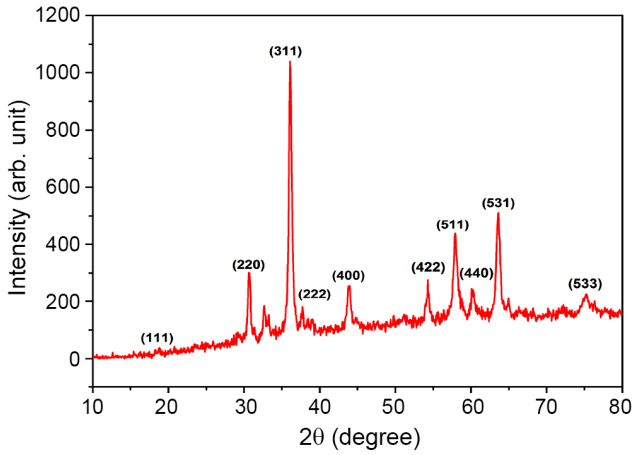

Fig. 1. XRD pattern of $CuMn_2O_4$ nanostructures calcined at 600°C for 4 h.

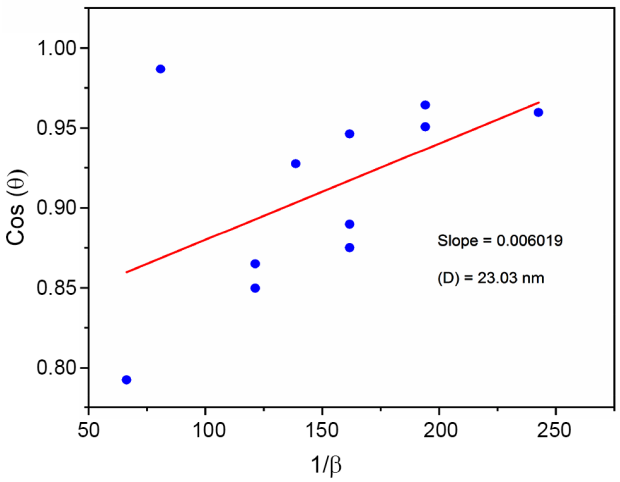

Fig. 2. Diagram of cosθ vs. 1/β using Scherrer equation.

The highest peak is at a diffraction angle of 36.1°. Several other tall peaks were also observed which agree with the diffraction pattern of the $CuMn_2O_4$ reference sample. As shown in Fig. 1, the characteristic peaks of $CuMn_2O_4$ are at the 2θ angles of 18.63 °, 30.69 °, 32.68 °, 36.1 °, 37.69 °, 43.88 °, 54.26 °, 57.91°, 60.23 °, 63.54 °, 75.10 °, respectively. The mean crystallite size of $CuMn_2O_4$ nanostructures was calculated using XRD pattern and Scherrer equation (Eq. 1):

$$D = \frac{K\lambda}{B\cos\theta} \quad (1)$$

where, D is the mean size of nanostructures, K = 0.9 is a crystallite shape factor for the spherical nanostructures, λ is the wavelength of 0.15418 nm, β is the full width at half the maximum and θ is the peak position.

The graph of 1/β on the X-axis and cosθ on the Y axis is shown in Fig. 2. Using the slope of the line of this equation, the mean size of the nanostructures was about 23.03 nm.

Evaluation of activation energy and kinetic properties

Thermal properties, either thermal degradation or calculation of the activation energy of the degradation process was favorite for estimation the thermal properties of $CuMn_2O_4$ nanostructures. The activation energy of degradation (Ed) was determined using TPR thermograms by Kissinger equation (Eq. 2) [21]:

$$\frac{-\ln\beta}{T_{Max}^2} = \frac{Ed}{RT_{Max}} - \frac{\ln AR}{Ed} \quad (2)$$

Where, β is the heating rate in °C/min, T_{Max} is the highest thermal peak, Ed is the activation energy, R is the gas constant, and A is a pre-parameter value. A plot of $1000/T_{Max}$ versus Ln β/T^2_{max} is a straight line and E_d is obtained from the graph slope. In this method, the activation energy is calculated without the need for the identification of the mechanism and the degree of chemical reaction. This method of measurement is applicable to thermally stable materials such as pigments, metal oxides, nano-composites [2,22,23]. The TPR is a relatively new method for the characterization of solids and is one of the most widely used quantitative techniques for investigating the reduction behavior of catalysts [24]. In this study, the TPR was studied in the temperature range of 1 to 900°C. Fig. 3 (a-d) shows the TPR analysis of $CuMn_2O_4$ nanostructures at three heating rates of 10, 15 and 20°C/min and Kissinger equation, respectively. In this experiment, a TPR/TPD device (SWORD Nano factory) and Kissinger equation were used to measure the activation energy. Thus, a mixture of H_2/Ar passes through the solid sample of $CuMn_2O_4$ nanostructures (0.30 g) and reacts with the structural oxygen of the sample during the heating operation. At the same time, the sample temperature rises at a linear rate. Due to the use of hydrogen in this process, a signal is recorded from the device, indicating the reduction rate of the test sample. In Fig. 3 (a), the sample shows no reduction below 425°C at a heating rate of 10°C/min, indicating very pure nanostructures. The highest thermal peak at 425°C indicates the highest reaction rate at heating rate of 10°C/min.

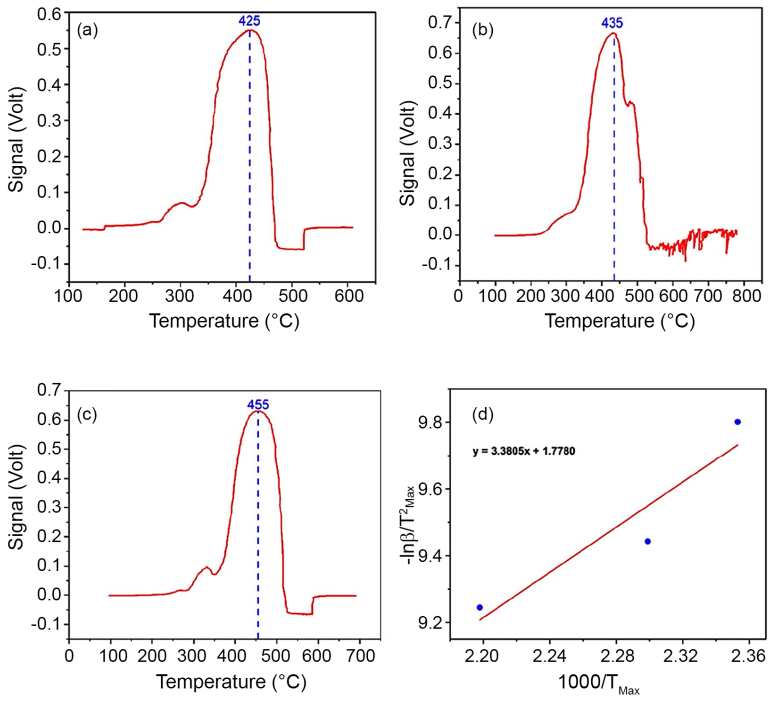

Fig. 3. TPR analysis of $CuMn_2O_4$ nanostructures at (a) 10°C/min, (b) 15°C/min, (c) 20°C/min and (d) Kissinger Equation and activation energy of $CuMn_2O_4$ nanostructures.

Table 1 summarizes the data of the highest thermal peaks indicating the highest reaction rate at all three heating rates. Also, T_{Max} 1000 versus Ln β/T^2_{Max} is placed in the Kissinger equation (Eq. 3), which created a straight line. The slope was calculated and the activation energy value was obtained 28.1 kJ/mol. Also, the activation energy value was 61.2 kJ/mol for Mn_2O_3 and 18 kJ/mol for CuO. A comparison of these three measured energy values showed that the activation energy is approximately the intermediate between the two other activation energy values [25, 26].

$$\ln\left(\frac{\beta}{T^2_{Max}}\right) = K + \frac{\frac{E_a}{R}}{\frac{1}{T_{Max}}} \qquad (3)$$

Magnetic characterization of $CuMn_2O_4$ nanostructures

Studies on copper oxide (CuO) nanoneedle using hydrothermal method have been shown ferromagnetic properties. The coercivity of CuO nanoneedles at 3 K in Oe, was estimated to be 42 Ω [27, 28]. Fig. 4 shows a VSM analysis of the hysteresis curve of $CuMn_2O_4$ nanostructures after heat treatment at 600°C. The results show the moderate ferromagnetic properties of these nanostructures. According to the M-H (magnetic field - magnetic charge) diagram, the saturation magnetization (M_s) is equal to 0.7 emu/g, the magnetic remanence (M_r) is approximately 0.1 emu/g, and the coercivity (H_c) is approximately 330 Oe. In addition,

Table 1. Summary of the highest thermal peaks of $CuMn_2O_4$ nanostructures according to Fig. 3 (a-c).

TPR Analysis	B (°C/min)	T_{Mas})°C
a	10	425
b	15	430
c	20	432

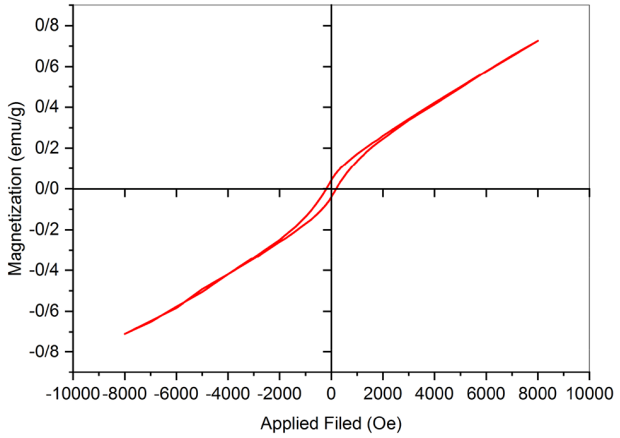

Fig. 4. Hysteresis curve of $CuMn_2O_4$ nanostructures calcined at 600 °C for 4 h.

according to the data from this diagram and the existence of a hysteresis loop or Mr, the results show the moderate ferromagnetic properties of $CuMn_2O_4$ nanostructures.

LCR test: Inductance, capacitance and resistance analysis

The LCR meter is used to measure the properties of a dielectric material [29]. Fig. 5 (a-d) shows the capacitance, quality factor, electrical conductivity, and electrical resistivity of $CuMn_2O_4$ nanostructures, respectively at different frequencies. Fig. 5(a) shows the electrical capacity diagram at a voltage of 10 mV and at 40 different frequencies (1 kHz-1000 kHz) using the LCR meter. The capacitance is calculated in accordance with the Eq. 4:

$$C = \frac{K_{\varepsilon_0 A}}{d} \quad (4)$$

Where, K is the dielectric constant and varies for each material. Approximately, K = 1 for air and ε_0 is the vacuum permeability that is 8.85×10^{-12} F/m. A is the capacitance area in m^2, d is the distance between the two capacitors plates in m and C is the capacitance in farad [30]. Empirical data show that the sample capacity at a constant voltage of 10 mV decreases with increasing in frequency. The highest electrical capacity in frequency of 1 kHz is equal to 3. Also, the electrical capacity decreases sharply in the frequency range of 26-100 kHz. The electrical capacity gradually decreases with a regular trend with increasing frequency in the range of 100-1000 kHz, and the highest capacity reduction is in the frequency of 1000 kHz.

Fig. 5(b) displays the diagram of the quality factor at a constant voltage of 10 mV at 40 frequencies from 1-1000 kHz using a LCR meter. The results show a direct relationship between the increasing in frequency and the quality factor as the sample quality factor increases with increasing frequency. The sample quality factor increases uniformly in the frequency range of 1-420 kHz. At frequencies of 420-600 kHz, a slight increase and decrease is observed. The highest quality factor increases is in the frequency range of 948-1000 kHz. The results indicating that the nanostructures can be used in the electronics industry because of their high-quality factor.

Fig. 5(c) shows the diagram of the electrical conductivity at a constant voltage of 10 mV at 29 frequencies from 200-1000 MHz using the LCR meter. The results show that the conductivity decreases with increasing

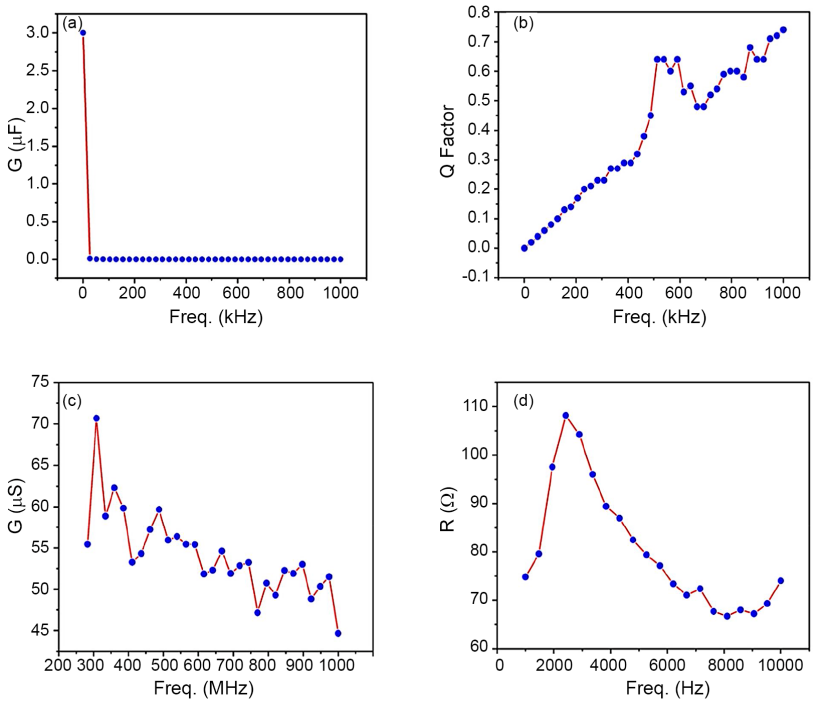

Fig. 5. (a) Capacitance, (b) quality factor, (c) electrical conductivity and (d) electrical resistivity of $CuMn_2O_4$ nanostructures.

frequency. The highest conductivity decrease was in the frequency of 1000 MHz and the highest conductivity increase was in the frequency of 308 MHz equal to 70.7 μS. In the frequency range of 400-1000 MHz, the conductivity decreases at a relatively constant rate, indicating the semiconducting property of these nanostructures.

Fig. 5(d) presents the diagram of the electrical resistance at a constant voltage of 10 mV at 20 frequencies from 1000-10000 Hz using the LCR meter. The results show that the highest electrical resistance is in the frequency of 2421 Hz. Electrical resistance decreases regularly with increasing frequency. The highest decrease in electrical resistance is in the frequency of 8000 Hz equal to 67 Ω.

CONCLUSION

In this study, the $CuMn_2O_4$ nanostructures was prepared by stearic acid sol-gel synthesis method. In the XRD pattern analysis, the mean size of $CuMn_2O_4$ nanostructures was measured to be 23.03 nm by Scherrer equation. The activation energy value of these nanostructures was 28.1 kj/mol using TPR analysis, Kissinger equation and obtaining a linear slope of equation. The results of VSM analysis showed the moderate ferromagnetic property of these nanostructures. In the LCR analysis, the highest electrical capacity was 3 μF in the frequency of 1 kHz and the highest quality factor was observed with increasing frequency in the range of 948-1000 kHz. The highest conductivity increase was in the frequency of 308 MHz equal to 70.7 μS. In addition, the highest decrease in electrical resistance was in the frequency of 8000 Hz equal to 67 Ω, indicating the semiconducting property of these nanostructures. Therefore, $CuMn_2O_4$ nanostructures can be used in the electronics and fuel cell industries.

REFERENCES

[1] West, A.R. (2009). Solid state chemistry and its applications, Wiley, Vol. 41, No. 6.

[2] Enhessari, M., Salehabadi, A., Khoobi, A., Amiri, R. (2017). Kinetic properties and structural analysis of $LaCrO_3$ nanoparticles. Mater. Sci. Poland, 35, 368-373.

[3] Zhang, L., Gu, F.X., Chan, J.M., Wang, A.Z., Langer, R.S., Farokhzad, O.C. (2008). Nanoparticles in medicine: therapeutic applications and developments. Clin. Pharmacol. Ther., 83, 761-769.

[4] Yousaf, M., Saeed, M. A., Isa, A.R.M., Shaari, A. H., Aliabad, A. R. (2012). Electronic Band Structure and Optical Parameters of Spinel $SnMg_2O_4$ by Modified Becke-Johnson Potential. Chinese Phys. Lett., 29, 107401.

[5] Salker, A. V., Gurav, S.M. (2000). Electronic and catalytic studies on Co1-xCuxMn_2O_4 for CO oxidation. J. Mater. Sci., 35, 4713-4719.

[6] Mohanta, S., Kaushik, S. D., Naik, I. (2019). Coexistence of spincanting and metamagnetism in tetragonal distorted spinel $CuMn_2O_4$. Solid State Commun., 287, 94-98.

[7] Chani, M.T.S., Karimov, K. S., Khan, S. B., Fatima, N., Asiri, A. M. (2019). Impedimetric humidity and temperature sensing properties of chitosan-$CuMn_2O_4$ spinel nanocomposite. Ceram. Int., 45, 10565-10571.

[8] Afriani, F., Ciswandi, Hermanto, B., Sudiro, T. (2018). Synthesis of $CuMn_2O_4$ spinel and its magnetic properties characterizations. in AIP Conference Proceedings, 1964, 20016.

[9] Parida, S. K., Mohapatra, J., Mishra, D. K. (2016). Structural and magnetic behavior of spinel $CuMn_2O_4$ synthesized by co-melting technique. Mater. Lett., 181, 116-118.

[10] Ranjbar-Nouri, Z., Soltanieh, M., Rastegari, S. (2018). Applying the protective $CuMn_2O_4$ spinel coating on AISI-430 ferritic stainless steel used as solid oxide fuel cell interconnects. Surf. Coatings Technol., 334, 365-372.

[11] Kalyani, P., Kalaiselvi, N. (2005). Various aspects of LiNiO2 chemistry: A review, Sci. Technol. Adv. Mater., 6, 689.

[12] Houshiar, M., Zebhi, F., Razi, Z. J., Alidoust, A., Askari, Z. (2014). Synthesis of cobalt ferrite ($CoFe_2O_4$) nanoparticles using combustion, coprecipitation, and precipitation methods: A comparison study of size, structural, and magnetic properties. J. Magn. Magn. Mater., 371, 43-48.

[13] Errandonea, D., Schwager, B., Ditz, R., Gess-

mann, C., Boehler, R., Ross, M. (2001). Systematics of transition-metal melting. Phys. Rev. B, 63, 132104.

[14]Suzuki, K., Kijima, K. (2005). Optical band gap of barium titanate nanoparticles prepared by RF-plasma chemical vapor deposition. Jpn. J. Appl. Phys., 44, 2081.

[15]Lei, Y., et al., (2013). Synthesis of porous carbon supported palladium nanoparticle catalysts by atomic layer deposition: application for rechargeable lithium-O_2 battery. Nano Lett., 13, 4182-4189.

[16]Xu, J., Yang, H., Fu, W., Du, K., Sui, Y., Chen, J., Zeng, Y., Li, M., Zou, G. (2007). Preparation and magnetic properties of magnetite nanoparticles by sol–gel method. J. Magn. Magn. Mater., 309, 307-311.

[17]Nejati, K., Zabihi, R. (2012). Preparation and magnetic properties of nano size nickel ferrite particles using hydrothermal method. Chem. Cent. J., 6, 23.

[18]Benito, G., Morales, M. P., Requena, J., Raposo, V., Vazquez, M., Moya, J.S. (2001). Barium hexaferrite monodispersed nanoparticles prepared by the ceramic method. J. Magn. Magn. Mater., 234, 65-72.

[19]Wright, J.D., Sommerdijk, N.A.J. M. (2014). Sol-gel materials: chemistry and applications. CRC press.

[20]Qiu, J., Gu, M. (2005). Magnetic nanocomposite thin films of $BaFe_{12}O_{19}$ and TiO_2 prepared by sol-gel method. Appl. Surf. Sci., 252, 888-892.

[21]Salehabadi, A., Abu Bakar, M. (2014). Kinetic and Nanomechanical Study of Poly (3-hydroxybutyrate)-Epoxidized Natural Rubber-Organomodified Montmorillonite Nanohybrids, 844, 229-234.

[22]Fathollahi, M., Mohammadi, B., Mohammadi, J. (2013). Kinetic investigation on thermal decomposition of hexahydro-1,3,5-trinitro-1,3,5-triazine (RDX) nanoparticles. Fuel, 104, 95-100.

[23]Blaine, R.L., Kissinger, H. E., (2012). Homer Kissinger and the Kissinger equation, Thermochim. Acta, 540, 1-6.

[24]Jones, A. (2014). Temperature-programmed reduction for solid materials characterization. CRC Press.

[25]Choi, S.W., Park, J.Y., Kim, S.S. (2011). Growth behavior and sensing properties of nanograins in CuO nanofibers. Chem. Eng. J., 172, 550-556.

[26]Saputra, E., Muhammad, S., Sun, H., Ang, H.M., Tadé, M. O., Wang, S. (2014). Shape-controlled activation of peroxymonosulfate by single crystal α-Mn_2O_3 for catalytic phenol degradation in aqueous solution. Appl. Catal. B Environ, 154, 246-251.

[27]Zhao, J. G., Liu, S. J., Yang, S. H. Yang, S. G. (2011). Hydrothermal synthesis and ferromagnetism of CuO nanosheets. Appl. Surf. Sci., 257, 9678-9681.

[28]Dar, M. A., Kim, Y. S., Kim, W. B., Sohn, J. M. Shin, H. S. (2008). Structural and magnetic properties of CuO nanoneedles synthesized by hydrothermal method. Appl. Surf. Sci., 254, 7477-7481.

[29]Sengodan, R., Shekar, B. C., Sathish, S. (2013). Morphology, structural and dielectric properties of vacuum evaporated V_2O_5 thin films. Phys. Procedia, 49, 158-165.

[30]Yao, B. Fang, Z.B., Zhu, Y. Y., Ji, T., He, G. (2012). A model for the frequency dispersion of the high-k metal-oxide-semiconductor capacitance in accumulation. Appl. Phys. Lett., 100, 222903.

AUTHOR (S) BIOSKETCHES

Morteza Enhessari, Associated Professor, Department of Chemistry, Naragh branch, Islamic Azad University, Naragh, Iran, *Email: enhessari@gmail.com*

Salahaddin Abdollah Lachini, Department of Chemistry, Mahabad Branch, Islamic Azad University, Mahabad, Iran